Materials and Design 181 (2019) 107920

Contents lists available at ScienceDirect

Materials and Design

journal homepage: www.elsevier.com/locate/matdes

Dynamic responses and energy absorption of hollow sphere structure subjected to blast loading

Fan Tang [a], Yanlong Sun [a], Zerong Guo [a], Wensu Chen [b], Mengqi Yuan [a,*]

[a] State Key Laboratory of Explosion Science and Technology, Beijing Institute of Technology, Beijing 100081, China
[b] Centre for Infrastructural Monitoring and Protection, School of Civil and Mechanical Engineering, Curtin University, Kent Street, Bentley, WA 6102, Australia

HIGHLIGHTS

- Lightweight hollow sphere structure was designed to reduce the weight by 37.7%~69.8%.
- Parametric study was carried out to improve the blast resistance of hollow sphere structure.
- The open-celled hollow sphere structure exhibited better blast resistance than the closed-cell hollow sphere structure.
- Blast-proof mechanism and blast resistance of hollow sphere structure was identified.

GRAPHICAL ABSTRACT

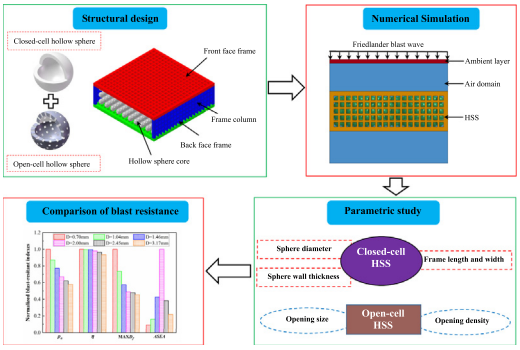

ARTICLE INFO

Article history:
Received 17 March 2019
Received in revised form 15 May 2019
Accepted 6 June 2019
Available online 8 June 2019

Keywords:
Closed-cell hollow sphere
Open-cell hollow sphere
Blast resistance
Parametric design
Numerical simulation

Data availability:
The raw/processed data required to reproduce these findings cannot be shared at this time as the data also forms part of an ongoing study.

ABSTRACT

Closed-cell and open-cell hollow spheres were designed to develop lightweight cellular structures with excellent blast resistance, and the mechanical response of the hollow sphere structure (HSS) under blast loading was investigated numerically using ANSYS®/LS-DYNA®17.0. In this paper, the blast wave pressure decay rate was served as the main index of blast resistance while areal specific energy absorption and frame deformation were used as auxiliary indexes. The results indicated that the weight of HSS was reduced by 37.7%–69.8% compared to solid structures with the same physical size, and the blast resistance of HSS was significantly affected by the hollow sphere diameter and wall thickness, frame length and width, opening size and opening density. Closed-cell HSS with smaller hollow sphere diameters and thicker wall, or smaller frame lengths and widths would achieve the optimal blast resistance. Meanwhile, the blast resistance of HSS could be improved by adopting a smaller opening size, but the effect of opening density did not follow any rule, which was affected by the number and position of openings. Comprehensively, the blast resistance of HSS was enhanced when there was opening only at the face blast surface rather than at both the face blast surface and back blast surface.

1. Introduction

The hollow sphere structure (HSS) is a type of foam structure that combines the structural characteristics of open-cell and closed-cell foams [1–3]. Compared to the existing open-cell and closed-cell

* Corresponding author at: Room 303, State Key Laboratory of Explosion Science and Technology, Beijing Institute of Technology, 5 South Zhongguancun Street, Haidian District, Beijing 100081, China.
E-mail address: myuan@bit.edu.cn (M. Yuan).

https://doi.org/10.1016/j.matdes.2019.107920

foams, the HSS has excellent mechanical performance and damping performance, high energy absorption rate and specific rigidity, low relative density and specific heat rate, and favorable damping and sound attenuation effects, which has been widely used in various areas, such as vehicle, rail transit and aerospace [4–7].

Most of the research on blast protection was focused on structures, such as aluminum foam, negative Poisson's ratio structure and high-performance fibers. Extensive efforts have been devoted to investigate mechanical properties and impact resistance of the hollow sphere, instead of blast protection [8–10]. For example, Gasser et al. [11] studied the effect of wall thickness and radius on the mechanical properties of the face-centered cubic HSS. Vesenjak et al. [12] found that the effect of topological structure and strain rate sensitivity on the impact resistance of HSS was significant, while the wall thickness did not, and the face-centered cubic arrangement had the best impact resistance. Zeng et al. [13] analyzed the effect of density gradient distribution on the mechanical response of hollow spheres under impact load and proposed that placing the "hardest" layer as the first layer and the "weakest" layer as the last layer to enhance the energy absorption rate of the sphere and reduce the force of the sphere structure on the protected structure. Li et al. [14] carried out the deformation mode and failure mechanism of the metal thin-walled hollow spheres under dynamic compression and found that the wall thickness-to-diameter ratio markedly affected the dynamic behavior of the sphere. Smith et al. [15] revealed the mechanical properties of HSS and identified several important mechanical parameters, such as compressive plastic Poisson's ratio, compressive unloading modulus, tensile unloading modulus, tensile yield stress and tensile fracture strain, etc. Shufrin et al. [16] found that the hollow sphere exhibited negative Poisson's ratio effect, and assemblies of spheres with the wall thickness to radius ratio smaller than 0.01 were able to provide the macroscopic Poisson's ratios close to −1.0. Yang et al. [17] analyzed the impact resistance of the gradient metal hollow sphere foam structure, found that the HSS with many gradients and negative gradients had the best impact resistance. Song et al. [18] investigated the effect of microporosity on the mechanical properties of the thin-walled hollow spheres, and found that the Young's modulus and yield strength of the spheres were unaffected by any increase in microporosity. Qi et al. [19] studied the blast resistance and multi-objective design optimization of aluminum foam-cored sandwich panels by using the maximum back face deflection and areal specific energy absorption as blast-resistant indexes.

There has been a wealth of research on the mechanical response, blast resistance and deformation mechanism of aluminum foam under blast loading. However, the structural parameters and arrangement of each aluminum foam cell are different, so they are difficult to change and optimize [20–22]. Compared with aluminum foam, the structural parameters and arrangement of hollow spheres are easier to be designed and optimized, and the uniformity of the hollow spheres could be achieved. It is worth noting that the effectiveness of HSS against blast loading is yet investigated and the blast-resistance behaviors and influencing factors are not well understood.

The closed-cell and the open-cell HSS were investigated in this paper. The ANSYS®/LS-DYNA® 17.0 finite element analysis software was used to study the effect of structural parameters of HSS on the blast resistance to enhance the blast resistance of the lightweight and high-strength blast-proof structure.

2. Finite element analysis

The finite element model (FEM) was established by Solidworks 2016, Hypermesh 2017, ANSYS®/LS-DYNA® 17.0 and LS-PrePost 4.3 software. Solidworks 2016 was used to build geometric models of HSS. Hypermesh 2017 was a pre-processing for meshing and setting of calculation parameters, so the element quality, calculation accuracy and convergence were guaranteed. ANSYS®/LS-DYNA® 17.0 was utilized for the calculation of FEM. LS-PrePost 4.3 was used to view and output the calculation results.

The FEM consisted of ambient layer, air domain and HSS, established in g-cm-μs unit, was shown in Fig. 1. In order to eliminate the effect of the diffraction blast wave on the transmission blast wave, the length and width of ambient layer and air domain remained the same as the frame. The heights of ambient layer and air domain were 0.5 mm and 59.5 mm, respectively. The distance between the ambient layer and the front surface of HSS was 30 mm. Meanwhile, the boundary conditions of ambient layer and air domain were set as shown in Fig. 1 to ensure that the Friedlander blast wave propagation in the air domain was stable. The ambient layer and air domain were modeled as hexahedral elements with the element size of 0.5 mm, and the Arbitrary Lagrange-Euler (ALE) approach was adopted. The HSS was meshed using hexahedral elements and the Lagrange approach was adopted. The fluid-structure interaction *CONSTRAINED_LAGRANGE_IN_SOLID was applied among the ambient layer, air domain and HSS. The contact between hollow spheres was defined as *CONTACT_ERODING_SINGLE_SURFACE, and the contact between hollow sphere core and frame was defined as *CONTACT_ERODING_SURFACE_TO_SURFACE.

2.1. Blast loading

In this study, the Friedlander method was used to simulate the dynamic responses of HSS subjected to blast loading. While the peak overpressure (1500 kPa) and the positive phase duration (1.0 ms) of blast wave were determined, the pressure-time (P-t) curve (Fig. 2a) of Friedlander blast wave could be expressed by Eq. (1) [23–25]. Then, the P-t curve was converted into internal energy-time (E-t) curve (Fig. 2b). Finally, the keyword *BOUNDARY_AMBIENT_EOS was used to load the internal energy-time (E-t) curve and the relative volume-time (V-t) curve (Fig. 2c) into the ambient layer to obtain Friedlander blast wave in the air domain.

$$P(t) = P_0 + P_+\left(1-\frac{t-t_a}{T_+}\right)e^{-\frac{b(t-t_a)}{T_+}} \tag{1}$$

where $P(t)$ is the blast wave overpressure as a function of time, P_0 is the ambient pressure, P_+ is the peak pressure of blast wave, T_+ is the positive phase duration, b is the time constant, t_a is the arrival time of blast wave.

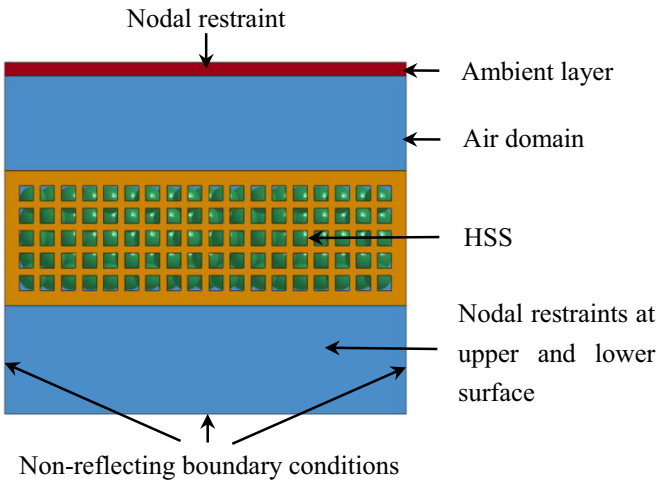

Fig. 1. Finite element model, and boundary conditions of the ambient layer and air domain.

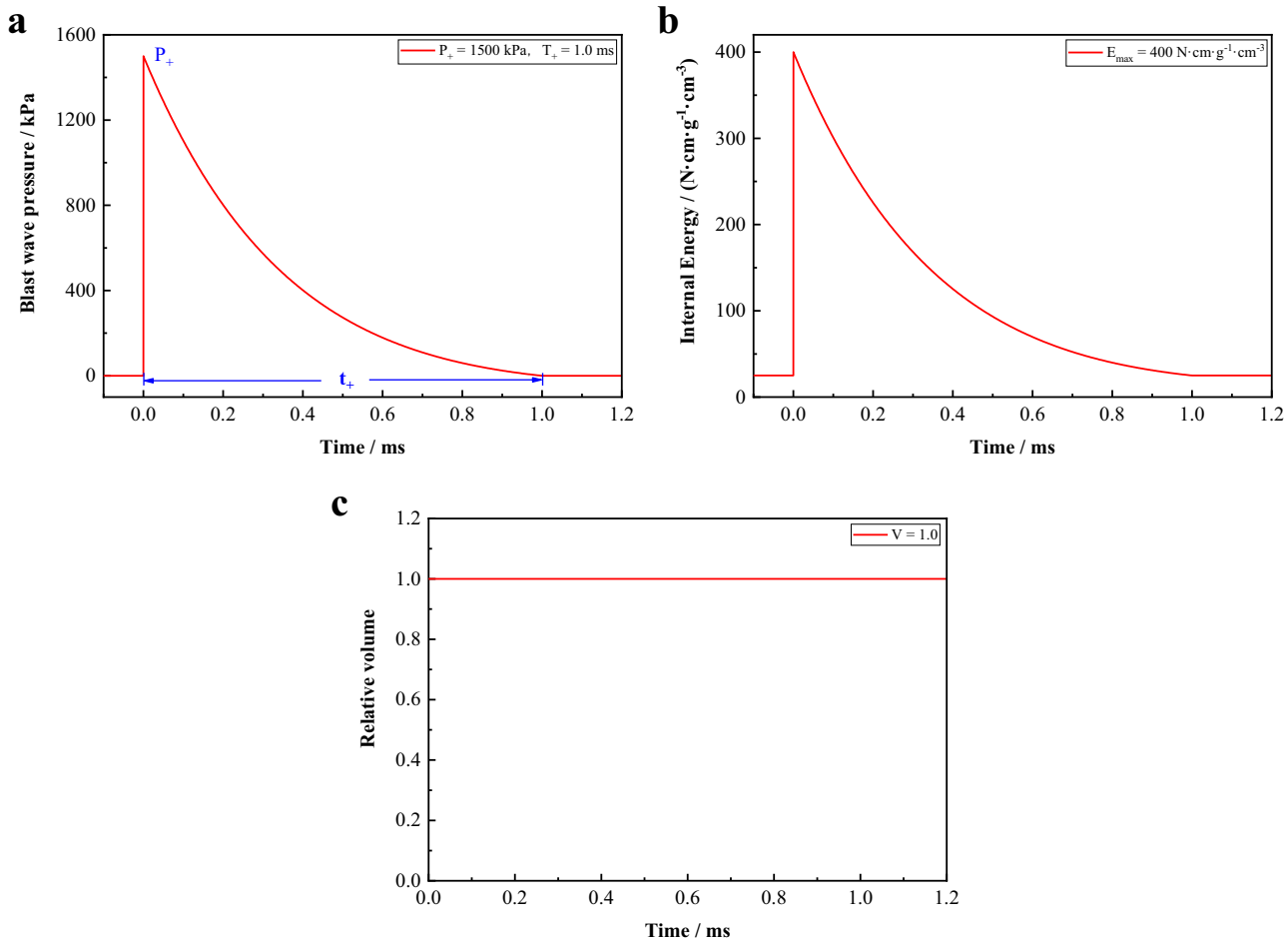

Fig. 2. Time histories of (a) pressure, (b) internal energy and (c) relative volume of incident Friedlander blast wave.

2.2. Geometric model of HSS

The HSS composed of a front face frame, frame column, back face frame and hollow sphere core, as shown in Fig. 3. A fully clamped frame was mounted outside the hollow sphere core, and the opening size of frame should be smaller than the hollow sphere diameter to prevent the hollow spheres from moving out of the frame. Meanwhile, the opening size of frame should not be too small to ensure that the blast wave could encounter the hollow sphere core. HSS shared the other geometric dimensions in the varied simulation conditions: thicknesses of front face frame (T_f = 1.13 mm) and back face frame (T_b = 1.13 mm), thickness of hollow sphere core (T_h = 7.74 mm) equals to the height of frame column (H = 7.74 mm), total thickness of HSS (T_{tot} = 10.00 mm), opening size of frame (A = 0.60 mm) and the size of frame beam section (B = 0.30 mm), as indicated in Figs. 3 and 4. The frame length (*L*) and width (*M*) are equal and range from 9.93 mm to 40.87 mm, as shown in Fig. 4.

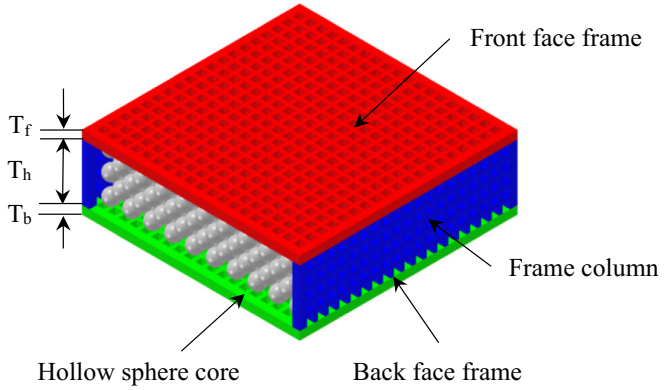

$T_f = T_b = 1.13$ mm, $T_h = 7.74$ mm, $T_{tot} = 10.00$ mm

Fig. 3. The schematic diagram of HSS.

The hollow sphere core was composed of a large number of hollow sphere with the same dimensions arranged regularly in the spatial periodicity. Its performance was affected by the spatial arrangement. Bravais [26] divided the space lattice structure into 7 major systems and 14 specific lattice structures. Among them, the face-centered cubic structure had superior energy absorption effects [27,28]. Therefore, the face-centered cubic arrangement of the hollow sphere core was used in the analysis (see Fig. 5). The closed-cell hollow sphere and open-cell hollow sphere were taken as the research object, as shown in Fig. 6(a–b). In the parametric study, the structural parameters of all hollow spheres were varied as shown in Tables 3–4, including hollow sphere diameter, hollow sphere wall thickness, layer of hollow sphere core, number of hollow spheres, opening size and opening density of hollow sphere. For open-cell HSS, there were four types of opening (see Fig. 7(a–d)): (a) open one hole at the face blast surface; (b) open one through-hole at the face blast surface and back blast surface; (c) open multiple holes at the face blast surface; (d) open multiple holes at the face blast surface and back blast surface.

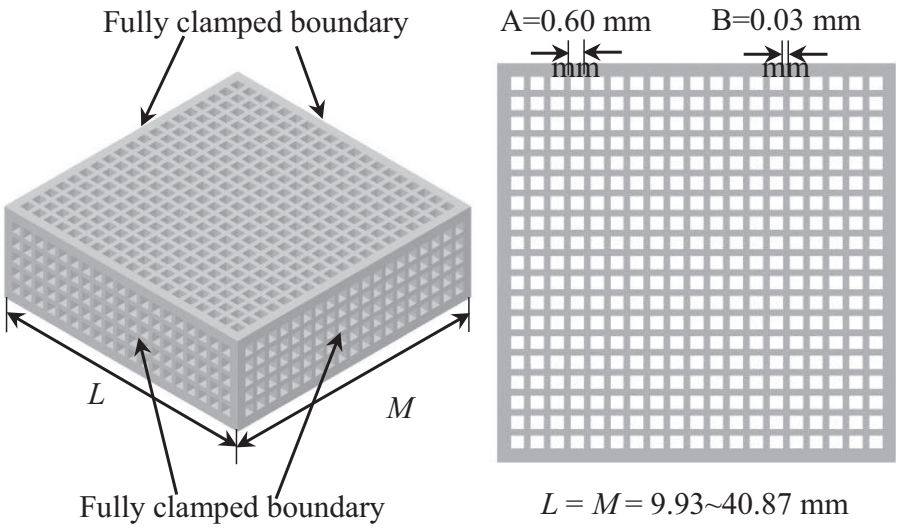

Fig. 4. The schematic diagram of frame.

2.3. Material model

The linear polynomial equation of state *EOS_LINEAR_POLYNOMIAL was applied on both the ambient layer and air domain. The blast wave pressure was expressed as Eq. (2).

$$P = C_0 + C_1\mu + C_2\mu^2 + C_3\mu^3 + (C_4 + C_5\mu + C_6\mu^2)E \tag{2}$$

$$\mu = \frac{1}{V} - 1 \tag{3}$$

where P is the blast wave pressure, E is the internal energy, V is the relative volume, ρ and ρ_0 are the present and initial densities of air, C_0, C_1, C_2, C_3, C_4, C_5 and C_6 are the 0th, 1st, 2nd, 3rd, 4th, 5th and 6th polynomial equation coefficients, respectively.

The material model *MAT_NULL was employed for the ambient layer and air domain. In addition, aluminum alloy $AlSi_{10}Mg$ was applied to construct the hollow sphere and frame in the simulation, and the elastic-plastic material model *MAT_PLASTIC_KINEMATIC was employed. The material parameters are given in Table 1 [29–31].

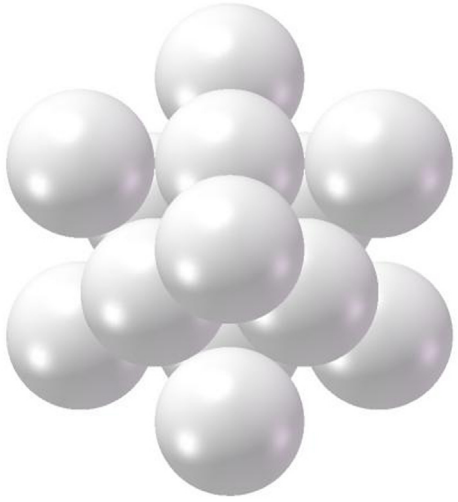

Fig. 5. The schematic diagram of face-centered cubic arrangement.

2.4. Validation of FEM

To validate the accuracy of Friedlander method and numerical model, structural response of aluminum foam sandwich panel (AFSP) under blast loading was simulated based on the experimental and numerical results of Zhu et al. [32]. The AFSP consisted of two layers of aluminum alloy (Al-2024-T3) and an aluminum foam core (Fig. 8). The TNT charge was 20 cm above the front face of AFSP.

The deformation of AFSP under blast loading was simulated with the LBE (LOAD_BLAST_ENHANCED) method and the Friedlander method. The blast loading of LBE method was defined by the keyword *LOAD_BLAST_ENHANCED, and the keyword *LOAD_BLAST_SEGMENT was applied to define the loading surface of ambient layer. First, the deformation process of AFSP was simulated by LBE method, and the blast wave pressure-time (P-t) curve loaded onto the AFSP was obtained. Then, the P-t curve obtained by the LBE method and V-t curve were applied to the ambient layer for simulating the Friedlander blast wave.

The blast wave impulse and maximum deformation of the back face was obtained by numerical simulation, as shown in Table 2. The maximum relative error of the blast wave impulse was 10.22% (LBE&Experiment), and the maximum relative error of the back face deformation was 6.67% (Friedlander&Experiment) and 9.25% (Friedlander&LBE). It could be found that the blast wave impulse and the maximum back face deformation obtained by Friedlander method were in good agreement with the results obtained by experiment [32] and LBE method. Therefore, the satisfactory correlations indicated that the adopted Friedlander method was valid.

3. Numerical results and discussion

The effect of hollow sphere diameter, hollow sphere wall thickness, frame length and width of closed-cell HSS, as well as the opening size and opening density of open-cell HSS on the blast resistance were investigated (see Tables 3–4). Fig. 9 showed the pressure-time curve of incident blast wave in front of HSS, with a peak overpressure of 1042.68 kPa, which was lower than the peak overpressure of loaded Friedlander blast wave (1500 kPa). The main reason was that the blast wave energy was attenuated when the blast wave propagates in the air. The termination time of FEM was set to 1.2 ms. First, the positive phase duration of incident blast wave was less than 1.0 ms. Second, the transmission blast wave pressure curve, and the energy and displacement curves of HSS had remained stable at 1.2 ms.

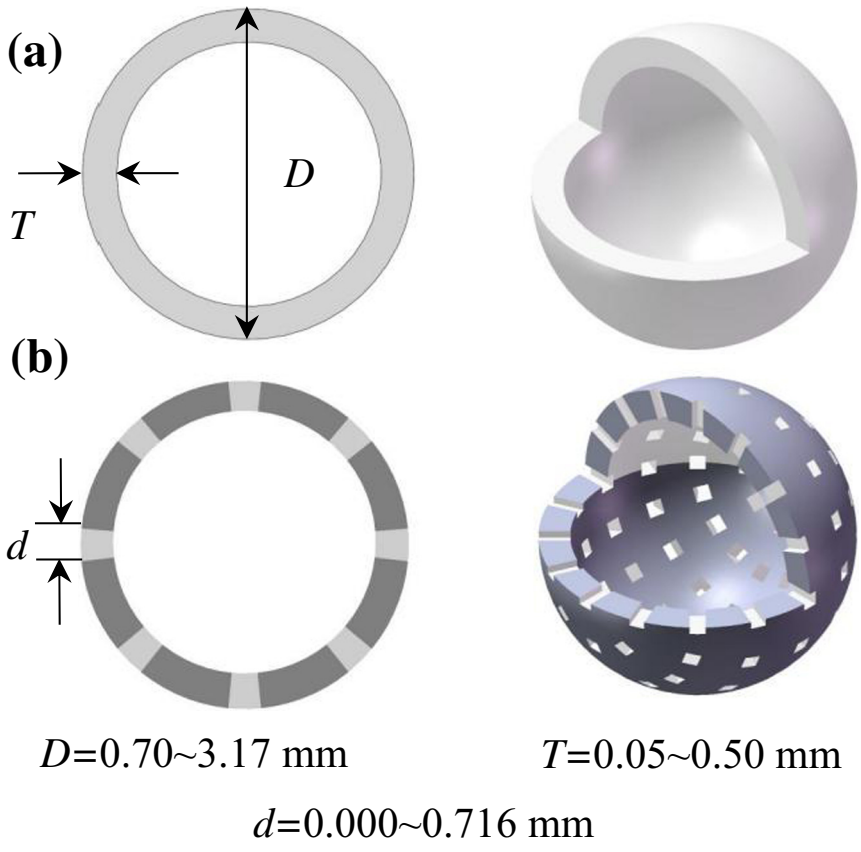

Fig. 6. The schematic diagram of (a) closed-cell hollow sphere and (b) open-cell hollow sphere.

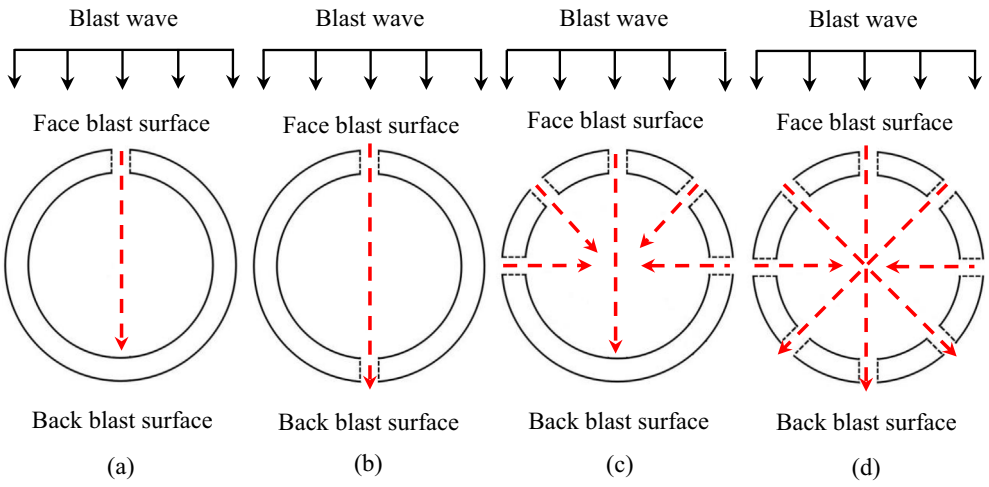

Fig. 7. Opening morphology of hollow sphere (a) open one hole at the face blast surface, (b) open one through-hole at the face blast surface and back blast surface, (c) open multiple holes at the face blast surface and (d) open multiple holes at the face blast surface and back blast surface.

Table 1
Material parameters of air and $AlSi_{10}Mg$ alloy [29–31].

Parameters	ρ_0 (kg/cm^3)	C_0/MPa	C_1	C_2	C_3	C_4	C_5	C_6	E_0/MPa	V_0
Ambient layer	1.29	−0.1	0.0	0.0	0.0	0.4	0.4	0.0	0.25	1.0
Air domain	1.29	−0.1	0.0	0.0	0.0	0.4	0.4	0.0	0.25	–

Parameters	Mass density/(g/cm^3)	Young's modulus/GPa	Yield stress/MPa	Poisson's ratio
$AlSi_{10}Mg$	2.65	70	251	0.32

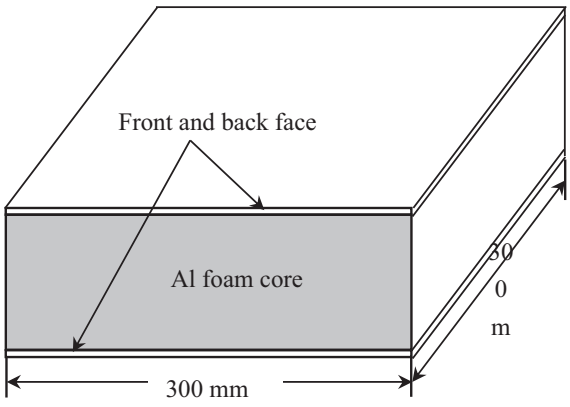

Fig. 8. The schematic diagram of aluminum foam sandwich panels.

3.1. Blast-resistant indexes of HSS

The areal density (ρ_a), blast wave pressure decay rate (η), maximum back face frame deformation (D_f) and areal specific energy absorption ($ASEA$) were used as blast-resistant indexes for the HSS performance after normalization [33–36]. The areal density (ρ_a) represents the mass within the unit area of the structure, and the total mass of the structure is lower when the areal density is smaller. The blast wave pressure decay rate (η) reflects the protective performance of HSS on blast wave. The maximum back face frame deformation reflects the buffered energy absorption of HSS when it is subjected to blast loading [37]. The areal specific energy absorption ($ASEA$) of HSS refers to the total energy absorbed by the mass per unit area, which not only reflects the energy absorption capacity, but also indicates the effect of areal density [38–41]. The areal density, blast wave pressure decay rate and areal specific energy absorption are expressed as Eqs. (4), (5) and (6).

$$\rho_a = \frac{m}{L^2} \tag{4}$$

$$\eta = \frac{P_I - P_T}{P_I} \times 100\% \tag{5}$$

$$ASEA = \frac{E_H}{\rho_a} \tag{6}$$

where m is the total mass of HSS, P_I is the incident blast wave pressure, P_T is the transmission blast wave pressure, and E_H is the total energy absorption of HSS.

Table 3
Parametric study of closed-cell HSS configuration on its blast resistance.

Structural parameters	Value					
D (mm)	**0.70**	**1.04**	**1.46**	**2.00**	**2.45**	**3.17**
ρ_a (g/cm^2)	1.65	1.45	1.29	1.12	1.03	0.96
n	15	10	7	5	4	3
N	5468	1445	424	203	98	38
Baseline	T = 0.20 mm L = 15.46 mm					
Nodes	1930	654	798	2886	2886	3960
Elements	1536	432	528	1920	1920	2636
T (mm)	**0.05**	**0.10**	**0.20**	**0.30**	**0.40**	**0.50**
ρ_a (g/cm^2)	0.80	0.92	1.12	1.27	1.39	1.47
Baseline	D = 2.00 mm L = 15.46 mm n = 5 N = 203					
Nodes	3076	2640	2886	2720	3010	3612
Elements	1536	1218	1920	2044	2400	3000
L (mm)	**9.93**	**15.46**	**21.06**	**29.60**	**40.87**	
ρ_a (g/cm^2)	1.21	1.12	1.08	1.06	1.04	
N	63	203	423	903	1823	
Baseline	D = 2.00 mm T = 0.20 mm n = 5					
Nodes	2886					
Elements	1920					

Table 4
Parametric study of open-cell HSS configuration on its blast resistance.

Structural parameters	Value							
d (mm)	**0.000**	**0.126**	**0.190**	**0.290**	**0.379**	**0.473**	**0.565**	**0.716**
ρ_a (g/cm^2)	1.12	1.118	1.118	1.117	1.115	1.113	1.107	1.098
Baseline	D = 2.00 mm T = 0.20 mm L = 15.46 mm n = 5 N = 203							
Nodes	2886	2886	2883	2880	2874	2850	2838	2811
Elements	1920	1918	1912	1908	1902	1880	1870	1848
$\boldsymbol{D_H}$ (‰)	**0.00**	**2.99**	**5.96**	**11.82**	**23.77**	**34.30**	**35.55**	**67.33**
ρ_a (g/cm^2)	1.12	1.118	1.115	1.113	1.108	1.103	1.102	1.089
Baseline	d = 0.19 mm D = 2.00 mm T = 0.20 mm L = 15.46 mm n = 5 N = 203							
Nodes	2886	2883	2880	2871	2859	2861	2859	2847
Elements	1920	1912	1904	1880	1856	1852	1848	1816

3.2. Blast resistance of closed-cell HSS

3.2.1. Effect of hollow sphere diameter on blast resistance

The effect of the hollow sphere diameters (D = 0.70–3.17 mm) on blast resistance was studied with the same baseline structural parameters: hollow sphere wall thickness (T = 0.20 mm), and frame length and width (L = 15.46 mm), while the layer of hollow sphere core (n = 3–15), and number of hollow spheres (N = 38–5468) were variable, as shown in Table 3.

Small element size and time step, and excellent element quality indicates improved calculation accuracy, but it also increases calculation time. Therefore, the scale factor for LS-DYNA computed time step is set to 0.6, and the number of elements and nodes are different for the HSS with different physical shapes. The hollow sphere was modeled as hexahedral elements, and the element size are selected based on the following standards: (1) the aspect ratio of element is close to 1.0, i.e. the

Table 2
Comparison of experimental and numerical results.

Configuration	*W* (g)	T_{FB} (mm)	T_{AF} (mm)	ρ_R (%)	Impulse/(N·s)		Back face deformation/mm		
					Experiment [32]	LBE	Experiment [32]	LBE	Friedlander
6.0%-20-20	20	1.0	20	6.0	18.29	16.42	4.90	5.04	5.13
6.1%-30-20	30	1.0	20	6.1	22.57	21.39	6.10	6.01	6.24
9.7%-20-20	20	1.0	20	9.7	18.08	16.42	4.40	4.63	4.57
9.8%-30-20	30	1.0	20	9.8	23.00	21.39	5.10	5.32	5.28
10.1%-30-30	30	1.0	30	10.1	22.36	21.39	2.40	2.27	2.48
9.9%-40-30	40	1.0	30	9.9	25.55	25.91	3.90	3.84	4.16

Configuration: Relative density of Aluminum foam - Mass of TNT charge - Aluminum foam core thickness.
W: Mass of TNT charge; T_{FB}: Front and back face thickness of AFSP.
T_{AF}: Aluminum foam core thickness; ρ_R: Relative density of Aluminum foam.

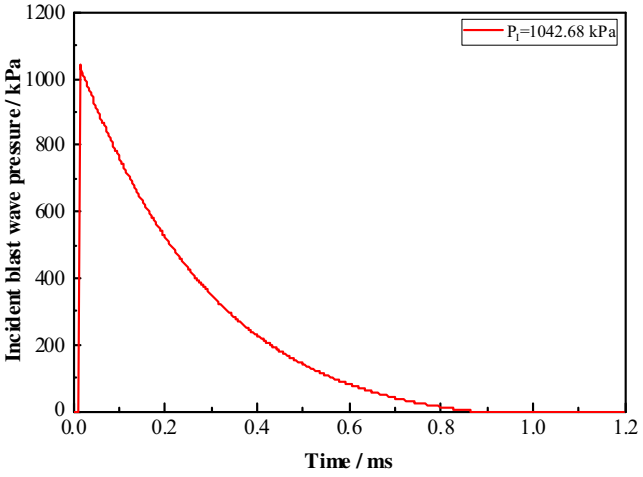

Fig. 9. Pressure-time curve of incident blast wave.

element is approximately a regular hexahedral; (2) the element size of hollow sphere must be able to ensure that the surface shape of the finite element model of hollow sphere is close to the real hollow sphere. The number of nodes and elements of single closed-cell hollow sphere are listed in Table 3. Comprehensively, the element size of the hollow sphere ranges from 0.025 mm to 0.1 mm, and the air are modeled as fixed hexahedral elements, of which the element size is 0.5 mm.

Fig. 10(a–c) shows the transmission blast wave pressure, the displacement of back face frame and the energy absorption of HSS under different hollow sphere diameters, and Fig. 11(a–d) compares the blast resistance with six sets of hollow sphere diameters. It could be observed that the areal density, the blast wave pressure decay rate, and the back face frame deformation all decreased as hollow sphere diameter increased. However, the total energy first increased and then decreased as hollow sphere diameter increased, and the total energy and *ASEA* were the largest at hollow sphere diameter of 2.00 mm. The areal density decreased by 4.18% from 1.65 g/cm^2 to 0.96 g/cm^2, the transmission blast wave pressure increased by 2652.92% from 2.57 kPa to 70.75 kPa, the maximum deformation of frame decreased by 54.40% from 0.182 mm to 0.083 mm and the *ASEA* change ranged from 0.86 J·cm^2·g^{-1} to 9.37 J·cm^2·g^{-1} as the diameter of hollow sphere increased by 352.86% from 0.70 mm to 3.17 mm.

When the hollow sphere diameter was less than 2.00 mm, with the decreasing hollow sphere diameter, the number of gaps in the HSS was larger, but the size of gaps was smaller. The deformation of the small-diameter hollow sphere was very small, the hollow sphere core was not fully compressed, and most of the energy was transmitted to the back face frame. So the hollow sphere core absorbed less energy and the frame experienced the majority of the deformation. The small-diameter HSS dispersed the blast wave into more gaps, thereby improving the capacity to attenuate blast wave energy. When the hollow sphere diameter was more than 2.00 mm, the number, layers and the total mass of hollow spheres decreased, resulting in a decrease in the amount of gaps in the HSS and an increase in the size of gaps. The blast wave was easily transmitted to the back of the structure through

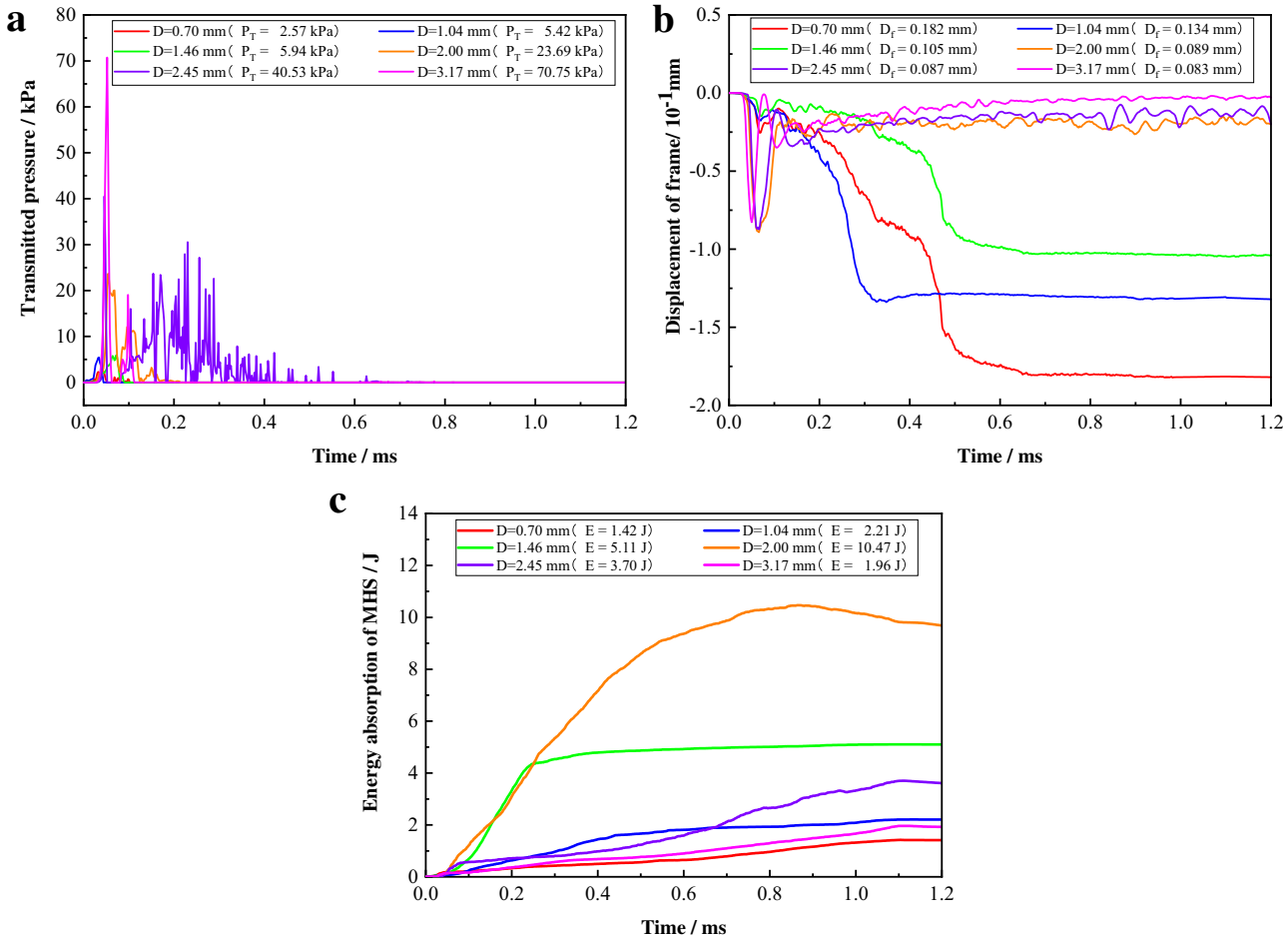

Fig. 10. Time histories of (a) transmission blast wave pressure, (b) back face frame deflection and (c) energy absorption under different hollow sphere diameters (*D*).

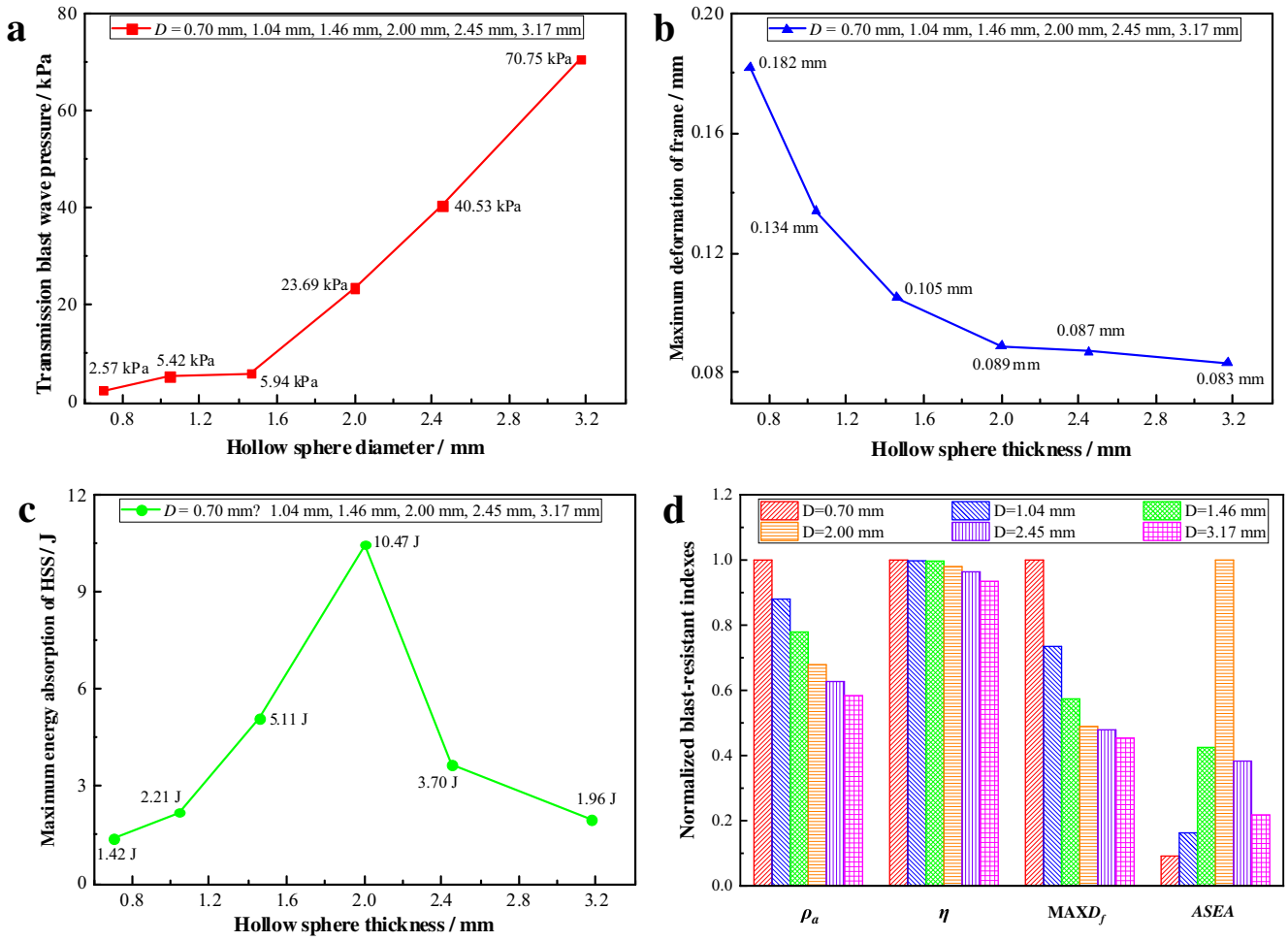

Fig. 11. Effect of hollow sphere diameter (D) on (a) transmission blast wave pressure, (b) back face frame deflection, (c) energy absorption and (d) normalized blast-resistant indexes.

the gaps, keeping the deformation of HSS fairly small and reducing the energy absorbed by the structure.

3.2.2. Effect of hollow sphere wall thickness on blast resistance

The effect of the hollow sphere wall thicknesses (T = 0.05–0.50 mm) on blast resistance was studied. HSS shared the same baseline structural parameters: hollow sphere diameter (D = 2.00 mm), frame length and width (L = 15.46 mm), layer of hollow sphere core (n = 5) and number of hollow spheres (N = 203).

The blast resistances with six kinds of hollow sphere wall thicknesses are presented in Fig. 12(a–d). It could be found that the greater the hollow sphere wall thickness was, the greater the HSS areal density, blast wave pressure decay rate, and back face frame deformation were. However, the total energy increased first and then decreased as hollow sphere wall thickness increased, and the total energy and *ASEA* were the largest when hollow sphere wall thickness was 0.30 mm. The areal density increased by 83.75% from 0.80 g/cm^2 to 1.47 g/cm^2, the transmission blast wave pressure decreased by 86.89% from 146.81 kPa to 19.24 kPa, the maximum frame deformation decreased by 22.11% from 0.104 mm to 0.081 mm and the *ASEA* ranged from 1.07 J·cm^2·g^{-1} to 13.56 J·cm^2·g^{-1} as hollow sphere wall thickness increased by 900.00% from 0.05 mm to 0.50 mm.

The hollow spheres with wall thicknesses of 0.10 mm and 0.05 mm exhibited much less blast resistance than the hollow spheres with a wall thickness exceeding 0.20 mm. This is mainly because thinner hollow sphere generates deformation much easier, which increases the gaps between the hollow spheres and allows blast waves to easily pass through the hollow sphere core, thereby reducing the blast resistance of HSS. Fig. 13 shows the deformation of the hollow spheres with a wall thickness of 0.05 mm. It can be seen that the hollow sphere experiences relatively large deformation. When the hollow sphere wall thickness exceeds 0.20 mm, the indexes of HSS do not change significantly because the deformations of the hollow sphere itself and the gaps between the hollow spheres are not obvious. Therefore, HSS with hollow sphere wall thicknesses of 0.20 mm, 0.30 mm, 0.40 mm, and 0.50 mm shared very similar blast-resistant performance.

3.2.3. Effect of frame length and width on blast resistance

The effect of the frame lengths and widths (L = 9.93–40.87 mm) on blast resistance was studied. HSS shared the same baseline structural parameters: hollow sphere diameter (D = 2.00 mm), hollow sphere wall thickness (T = 0.20 mm), layer of hollow sphere core (n = 5), while the number of hollow spheres (N = 63–1823) was variable.

As shown in Fig. 14(a–d), the frame length and width appear to have a significant effect on blast resistance of HSS. A larger frame length and width resulted in smaller areal density and blast wave pressure decay rate as well as greater total energy of structure and back face frame deformation. The areal density of HSS decreased from 1.21 g/cm^2 to 1.04 g/cm^2 by 14.05%, the transmission blast wave pressure increased by 1324.70% from 6.76 kPa to 96.31 kPa, the maximum deformation of the frame increased by 17,428.57% from 0.014 mm to 2.454 mm, and the *ASEA* increased by 35,754.55% from 0.11 J·cm^2·g^{-1} to 39.44 J·cm^2·g^{-1} as the frame length and width increased by 311.58% from 9.93 mm to 40.87 mm.

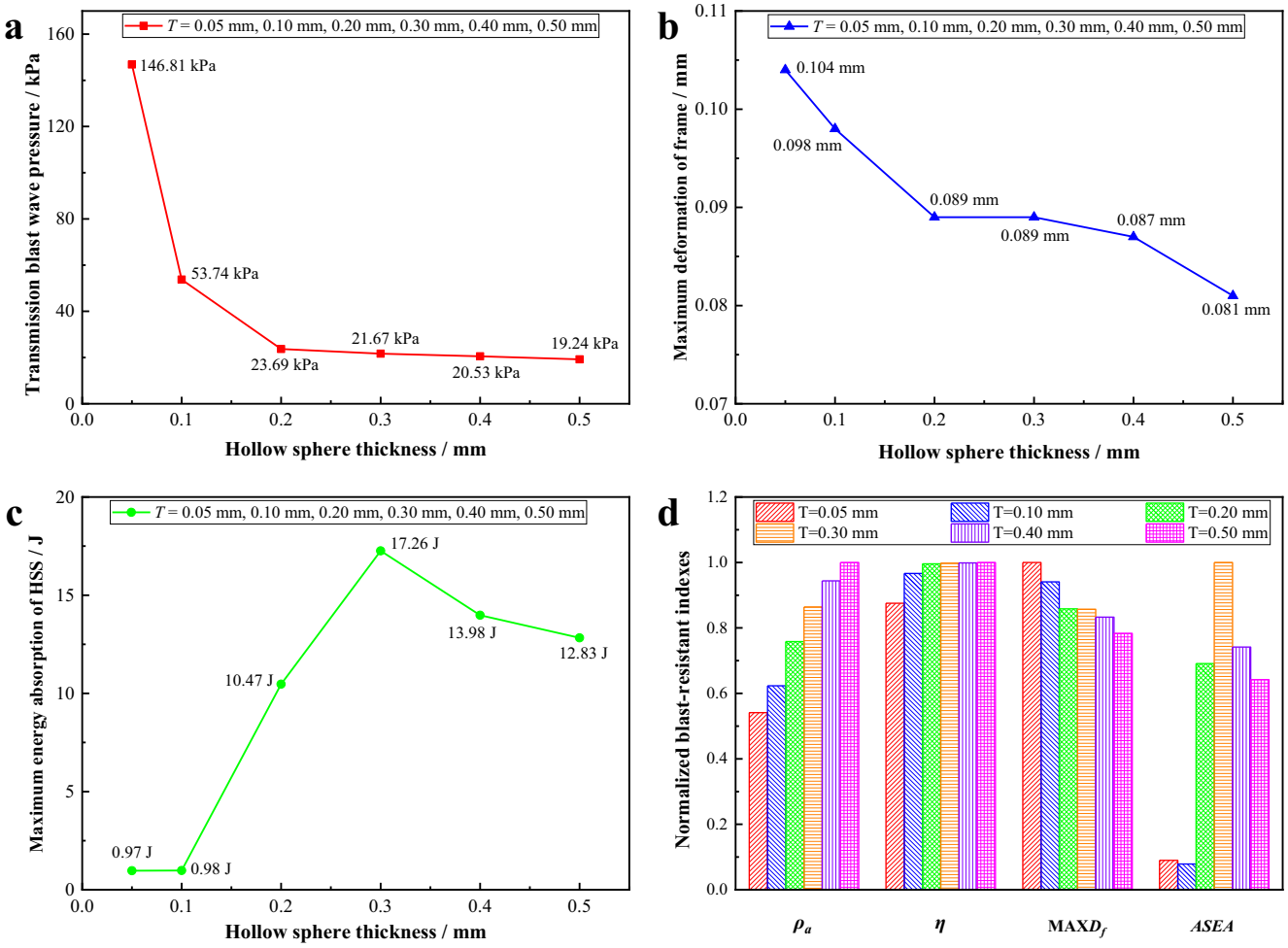

Fig. 12. Effect of hollow sphere wall thickness (T) on (a) transmission blast wave pressure, (b) back face frame deflection, (c) energy absorption and (d) normalized blast-resistant indexes.

The HSS had the most inferior blast resistance as the frame length and width increased because a larger frame was more easily deformed and created larger gaps between hollow spheres, causing the blast wave to pass through the hollow sphere core more easily.

3.3. Blast resistance of open-cell HSS

Based on the study of the areal density and blast resistance of the closed-cell HSS, the configurations of hollow sphere diameter of 2.00 mm, hollow sphere wall thickness of 0.20 mm and frame length and width of 15.46 mm were identified for the open-cell HSS, and the number of nodes and elements of single open-cell hollow sphere is listed in Table 4. Meanwhile, the entire open-cell HSS had the same baseline structural parameters: layer of hollow sphere core (n = 5), number of hollow spheres (N = 203). The open-cell structure composed of closed-cell hollow spheres by drilling square holes to examine the effect of opening size and opening density on the blast resistance of HSS. Opening density (D_H) can be expressed by Eq. (7).

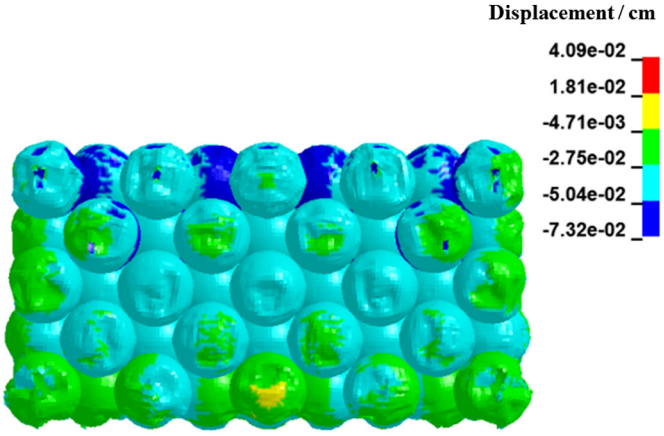

Fig. 13. Deformation of hollow sphere (T = 0.05 mm).

$$D_H = \frac{S_H}{S} \times 100\% \tag{7}$$

where S_H is the opening area, S is the external surface area of hollow sphere.

3.3.1. Effect of opening size on blast resistance

The effect of the opening sizes (d = 0.000–0.716 mm) on blast resistance was studied, as shown in Fig. 15(a–d). The blast wave pressure decay rate, frame deformation, total energy and *ASEA* varied throughout the simulation. The areal density ranged from 1.119 g/cm^2 to 1.096 g/cm^2, the transmission blast wave pressure ranged from 11.13 kPa to 31.55 kPa, the maximum deformation of the frame ranged from 0.062 mm to 0.090 mm and the structural *ASEA* ranged from 8.57 J·cm^2·g^{-1} to 10.08 J·cm^2·g^{-1} as the opening size increased 468.25% from 0.126 mm to 0.716 mm.

When the opening size of the hollow sphere is small, it is difficult for the blast wave to enter the inside of the hollow sphere through the

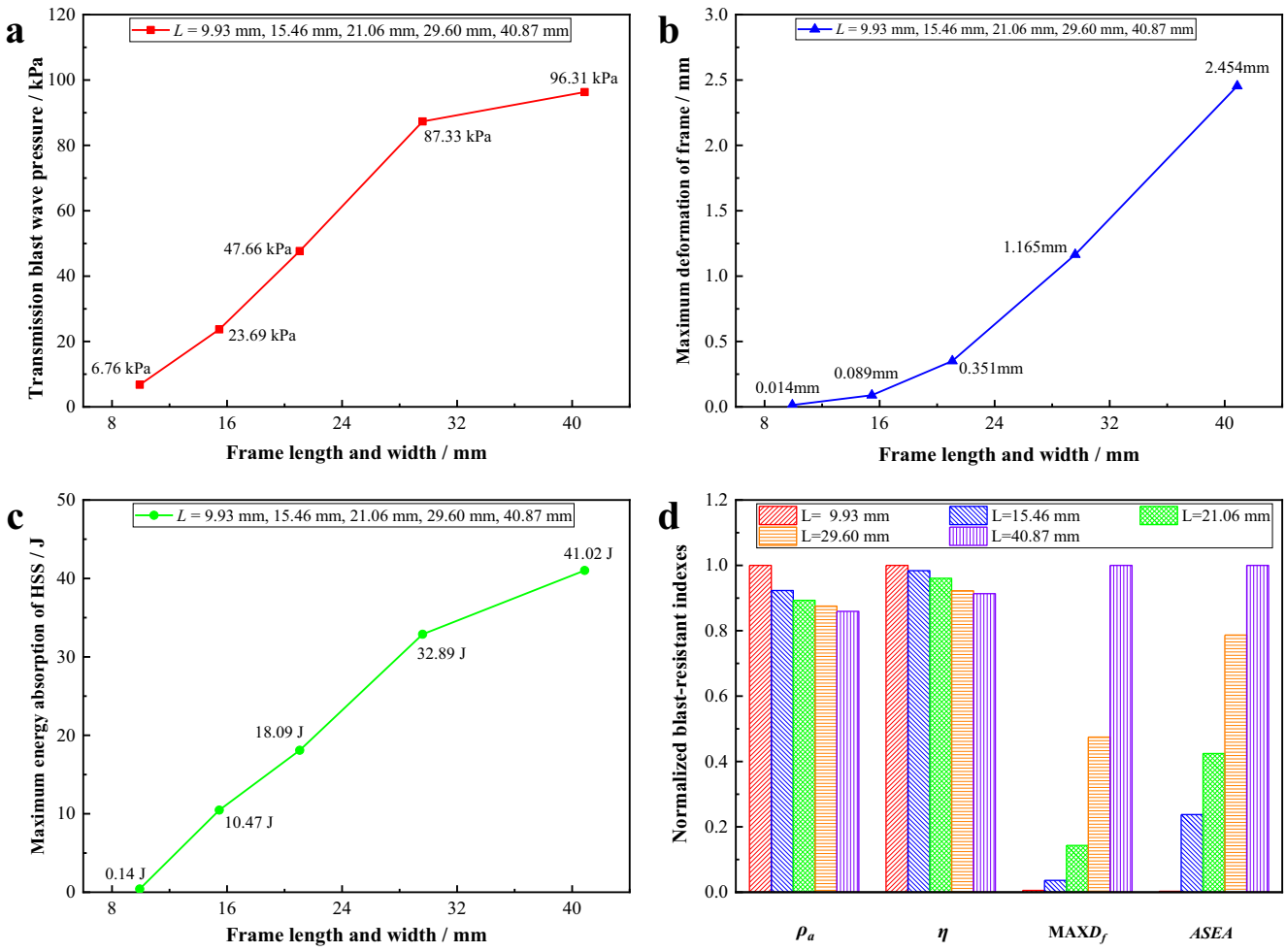

Fig. 14. Effect of frame size (L) on (a) transmission blast wave pressure, (b) back face frame deflection, (c) energy absorption and (d) normalized blast-resistant indexes.

opening. When the opening size of the hollow sphere is large, the hollow sphere is prone to deform and then damage. Large deformation enlarges the gap between the hollow spheres and makes it easier for blast wave to propagate into the hollow sphere core. The closed-cell hollow spheres are tangent arranged, so the arrangement between the open-cell HSS altered during the process, and enlarges the distance between the hollow spheres. Therefore, the open-cell hollow spheres are more easily misaligned than closed-cell spheres.

3.3.2. Effect of opening density on blast resistance

The effect of the opening density (D_H = 0.00–67.43‰) on blast resistance was studied. All open-cell HSS had the same opening density d = 0.190 mm. No obvious effect laws for opening density could be obtained from Fig. 16(a–d). It can be observed from Fig. 7(a–b) that the blast wave is more easily transmitted through the through-hole hollow sphere directly to the back of HSS. After the blast wave enters the hollow sphere through the opening, the energy dissipation only occurs inside the hollow sphere. Therefore, the blast resistance of HSS with one hole at the face blast surface (D_H = 2.99‰) is better than that of the through-hole structure (2 holes, D_H = 5.96‰) at the face blast surface and back blast surface. Similarly, according to Fig. 7(c–d), the blast resistance of the structure with multiple holes at the face blast surface (D_H = 34.30‰) is better than that with multiple holes at the face blast surface and back blast surface (D_H = 35.55‰ and D_H = 67.33‰). It is found that the opening size and opening density significantly affect the blast resistance, as does the opening location (D_H = 34.30‰ and D_H = 35.55‰). Therefore, the blast resistance of open-cell HSS is superior to the closed-cell HSS under certain conditions.

Three blast-resistant indexes were examined (blast wave pressure decay rate, areal specific energy absorption, and maximum deformation of back face frame), which essentially conflicted with each other and showed incongruent change laws [19]. The areal density of the structure and the stiffness of the hollow sphere increase. Therefore, the plastic deformation of the small-diameter hollow sphere was small, and the hollow sphere core was not fully compressed. Most of the energy was transmitted to the back face frame, resulting in a decrease in energy absorption of hollow sphere core and an increase in the deformation of the frame. Greater structural deformation generally results in more energy absorption. However, these two blast-resistant indexes (areal specific energy absorption and maximum back face frame deformation) were in conflict, which was consistent with the results obtained by Qi et al. [19]. In our case, the blast wave pressure decay rate should be used as the main evaluation index of structural blast-resistant performance in terms of its resistance against blast wave pressure [42].

3.4. HSS dynamic response process

When the HSS is subjected to blast loading, its dynamic response can be divided into four phases. The starting and ending moments of each phase are slightly different for different HSS. Figs. 17(a–e) and 18(a–b) show the deformation and stress distribution of HSS at various time slots, as well as time histories of front face frame and back face frame

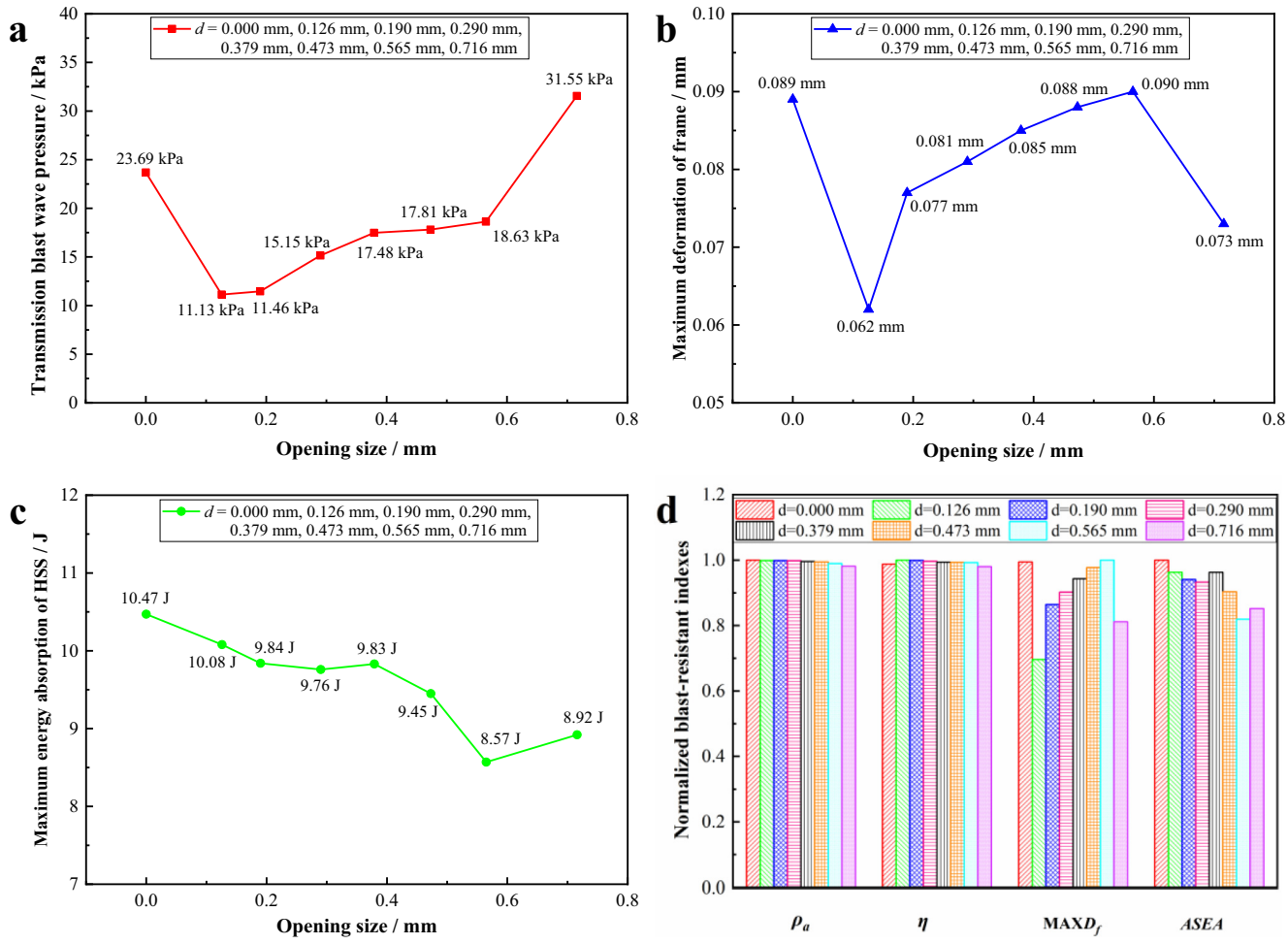

Fig. 15. Effect of hollow sphere opening size (d) on (a) transmission blast wave pressure, (b) back face frame deflection, (c) energy absorption and (d) normalized blast-resistant indexes.

deformation, of which the hollow sphere diameter is 2.00 mm, the hollow sphere wall thickness is 0.20 mm, the frame length and width is 15.46 mm, the layer of hollow spheres is 5 with a total of 903 hollow spheres.

Phase I (0–30 μs): The HSS is not deformed before the HSS is subjected to the blast wave, as shown in Fig. 17(a). When the blast wave is applied to the front face frame, the front face frame starts to deform and generates a certain initial velocity. The hollow sphere core is compressed by the front face frame, while the back face frame remains almost stationary, as shown in Fig. 17(b).

Phase II (30–164 μs): Due to the combined effects of the hollow sphere core movement and the blast wave applied on the back face frame, the back face frame starts to deform and the front face frame continues to compress the hollow sphere core until the back face frame reaches its maximum deformation. The hollow sphere core produces severe compression and deformation resulting in a sizable change in the spatial position of the hollow spheres and in the arrangement of the hollow spheres, as shown in Fig. 17(c).

Phase III (164–270 μs): With the constant decay of the incident blast wave pressure, the stretched front face frame, back face frame as well as the compressed hollow sphere core start to rebound. After the impact of the blast wave on the HSS, the bulging phenomenon occurs on the front face frame. When the blast wave propagates inside the hollow sphere core, the reflection pressure is generated due to the reflection by the back layer hollow spheres. Therefore, the front layer hollow spheres start to move in reverse under the action of the reflection pressure, resulting in a bulge on the front face frame and a positive displacement, as shown in Figs. 17(d) and 18(a).

Phase IV (270–1100 μs): When the frame and the hollow sphere core rebound to a certain extent, the front face frame begins to vibrate near the equilibrium position while the back face frame remains relatively stable and plastic deformation occurs, as shown in Figs. 17(e) and 18(b).

3.5. Energy absorption properties of HSS

Fig. 19 shows the energy absorbed by various parts of HSS, where the energy absorbed by the hollow sphere core accounts for 98.40% of the total energy absorbed by the HSS, and the internal energy accounts for 81.57% of the total energy. However, the energy absorbed by the frame accounts for 1.60% of the total energy absorbed by the HSS, and the internal energy accounts for 99.81% of the total energy. Therefore, the energy absorbed by the hollow sphere core is much higher than the energy absorbed by the frame. It is because the energy absorbed by the hollow sphere core is derived from the deformation of a large number of hollow spheres, and the energy absorbed by the frame is mainly derived from the deformation of the front face frame and the back face frame. The deformation of the back face frame mainly depends on the overall compression of the hollow sphere core and the impact of the blast wave, which mainly indicate the overall displacement of the hollow sphere core along the direction of the blast wave propagation; that is, the larger overall displacement of the hollow sphere core as a

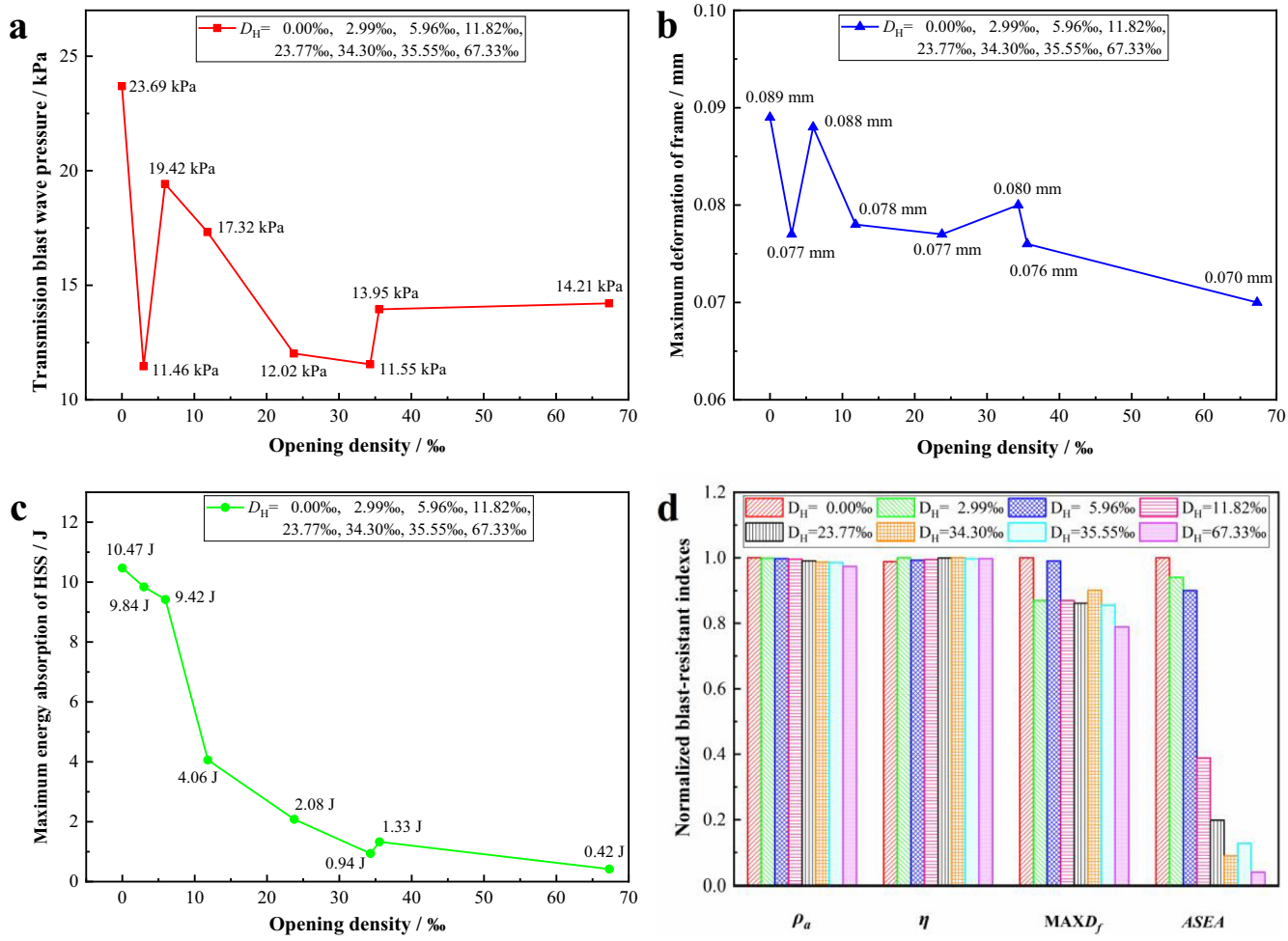

Fig. 16. Effect of hollow sphere opening density (D_H) on (a) transmission blast wave pressure, (b) back face frame deflection, (c) energy absorption and (d) normalized blast-resistant indexes.

total, does not indicate that all of the hollow sphere cells have larger deformation. Therefore, the maximum back face frame deformation does not sync with the maximum energy absorption of HSS.

The time histories of pressure along the blast wave propagation direction are displayed in Fig. 20. The incident blast wave pressure is 1042.68 kPa, the reflected blast wave pressure in front of the front face frame is 3507.79 kPa, the blast wave pressure inside the hollow sphere core is 588.53 kPa (3 mm from the front face frame) and 288.95 kPa (6 mm from the front face frame), and the transmission blast wave pressure behind the back face frame is 87.33 kPa. It appears that the blast wave energy continues to decay when the wave propagation distance inside the HSS increases. Since the blast wave is reflected and diffracted by HSS and the deformation of HSS itself, the blast wave energy dissipation is evident. The blast wave is also superimposed inside the HSS and generates internal friction to drive blast wave propagates and attenuates in the HSS.

In the closed-cell hollow sphere, the blast wave is reflected and diffracted in the gaps among the hollow spheres while continually dissipating energy. When the blast wave interacts with the hollow spheres, the structure resonates and attenuates the blast wave energy through the deformation of HSS, as well as the reflection of the surface of the hollow sphere. In open-cell hollow spheres, the hole is opened on the surface so that the blast wave can enter into the spheres to increase the collision area between the blast wave and the wall of the sphere. The reflection and diffraction of the blast wave interior of the sphere and in the gaps among the hollow spheres is strengthened, thereby improving the structure's ability to attenuate blast wave energy [42].

4. Conclusion

In this work, the blast resistance, deformation models and energy absorption of HSS with closed-cell and open-cell hollow spheres were investigated numerically. Meanwhile, the areal density, blast wave pressure decay rate, maximum back face frame deformation and areal specific energy absorption of HSS were compared and analyzed. The conclusions can be summarized as follows.

(1) The HSS not only has light weight, but also exhibits excellent blast resistance. The areal density of the solid structures with the same physical size is 2.65 g/cm^2, but the maximum areal density and minimum areal density of the HSS is 1.65 g/cm^2 and 0.80 g/cm^2, so the weight of HSS is reduced by 37.7%–69.8% compared solid structures with the same physical size.
(2) The blast resistance of HSS is significantly affected by the hollow sphere diameter, wall thickness, frame length and width, opening size and opening density. The blast wave attenuation of the closed-cell HSS is more effective when the closed-cell hollow sphere diameter is smaller, the sphere hollow wall thickness is larger, or the frame length and width are smaller.
(3) The open-celled HSS generally yields better blast resistance compared with the closed-cell HSS under a certain opening size and

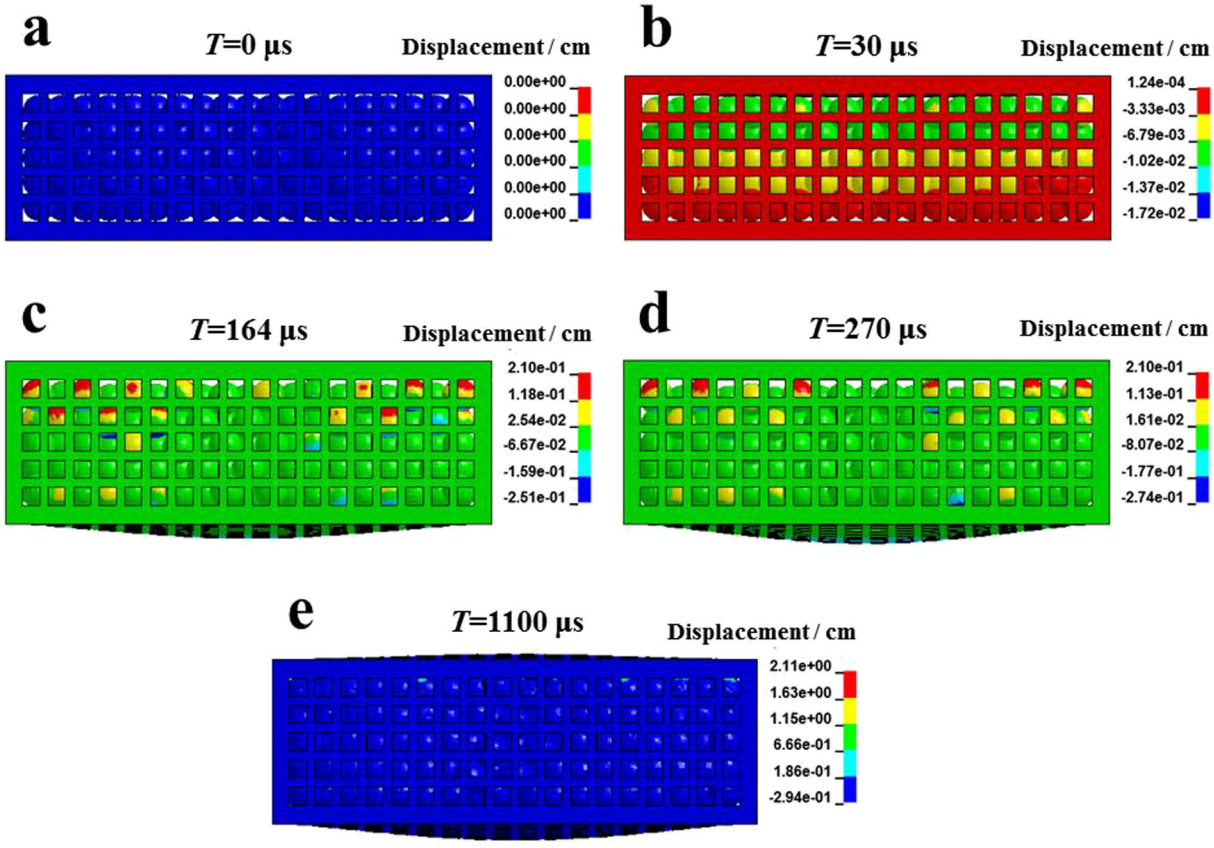

Fig. 17. Deformation and stress distribution of the HSS at (a) 0 μs, (b) 30 μs, (c) 164 μs, (d) 270 μs and (e) 1100 μs.

opening position. The blast resistance of HSS with open one hole at the face blast surface is superior to the blast resistance of HSS with open one through-hole along the blast wave propagation direction, and the blast resistance of the structure with open multiple holes at the face blast surface is better than that with open multiple holes at the face blast surface and back blast surface.

(4) The blast wave is mitigated by the HSS via the gaps between or inside the hollow spheres. Strong reflections and diffractions occur in the gaps, which cause resonance and deformation of HSS to mitigate blast wave.

Nomenclature

ASEA	Areal specific energy absorption
A	Opening size of frame
B	Size of frame beam section
b	Time constant
d	Opening size of hollow sphere
D	Hollow sphere diameter
D_H	Opening density of hollow sphere
D_f	Maximum back face frame deformation
E	Internal energy

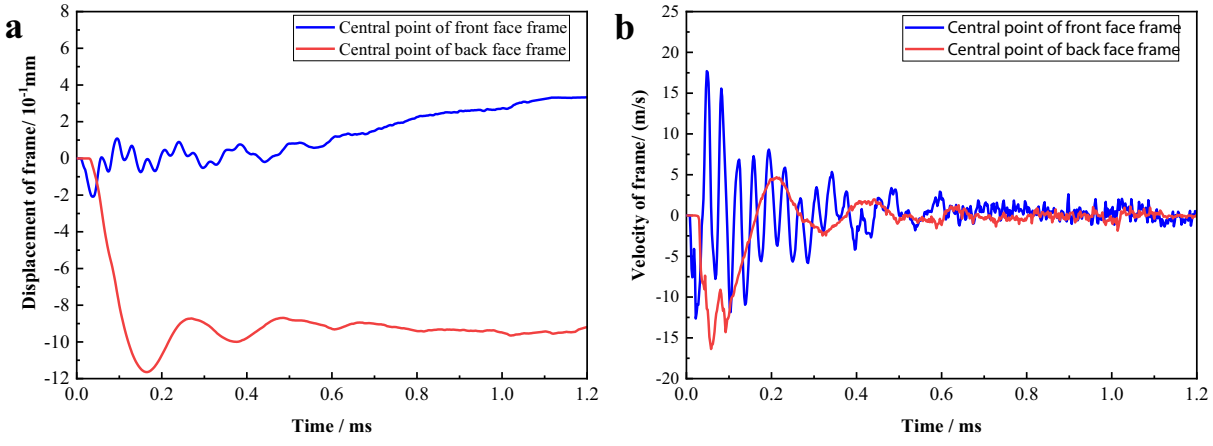

Fig. 18. Time histories of (a) deformation and (b) velocity of frame.

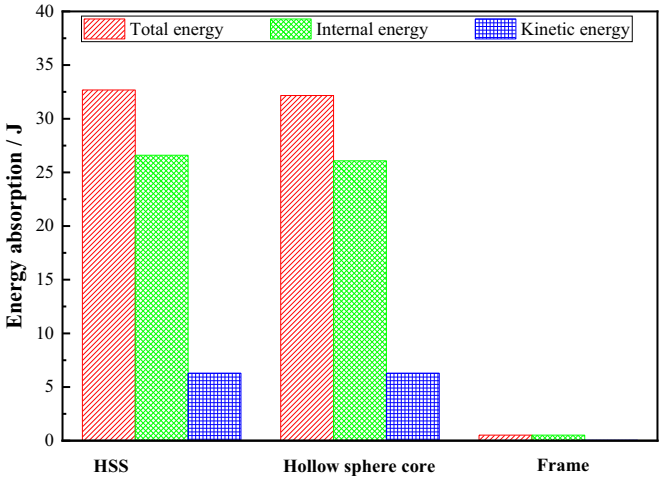

Fig. 19. Energy absorption of different parts of the HSS.

E_0 Initial internal energy
E_H Total energy absorption of HSS
H Frame column height
L Frame length
M Frame width
m Total mass of HSS
N Number of hollow spheres
n Layer of hollow sphere core
P Blast wave pressure
P_0 Ambient pressure
P_+ Peak pressure of blast wave
P_I Incident blast wave pressure
P_T Transmission blast wave pressure
S External surface area of hollow sphere
S_H Opening area of hollow sphere
t Time
T Hollow sphere wall thickness
T_+ Positive phase duration
T_f Thickness of front face frame
T_b Thickness of back face frame
T_h Thickness of hollow sphere core
T_{tot} Total thickness of HSS
T_{FB} Front and back face thickness of AFSP
T_{AF} Aluminum foam core thickness
V Relative volume
V_0 Initial relative volume
W Mass of TNT charge
ρ Density of air
ρ_0 Initial density of air
ρ_a Areal density
ρ_R Relative density of Aluminum foam
η Blast wave pressure decay rate
$C_0, C_1, C_2, C_3, C_4, C_5, C_6$ 0^{th}, 1^{st}, 2^{nd}, 3^{rd}, 4^{th}, 5^{th} and 6^{th} polynomial equation coefficients

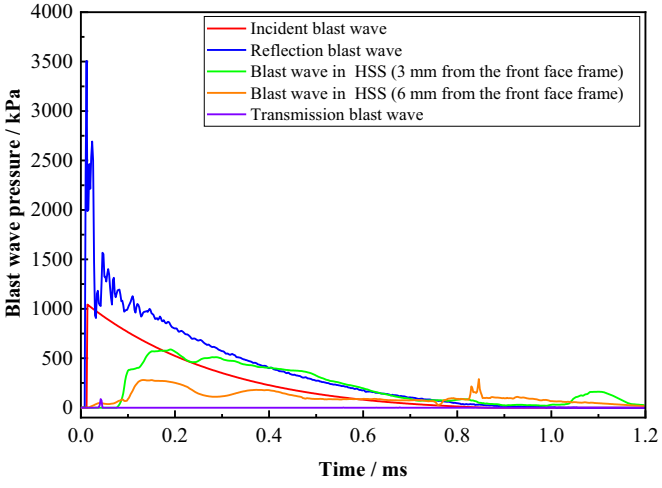

Fig. 20. Time histories of blast wave pressure.

CRediT authorship contribution statement

Fan Tang: Conceptualization, Formal analysis, Methodology, Software, Validation, Writing-original draft. **Yanlong Sun:** Conceptualization, Data curation, Investigation, Methodology, Visualization. **Zerong Guo:** Methodology, Resources, Supervision, Writing - review & editing. **Wensu Chen:** Methodology, Project administration, Software, Writing - review & editing. **Mengqi Yuan:** Funding acquisition, Project administration, Supervision, Writing - review & editing..

Declaration of Competing Interest

The authors declare that they have no conflict of interest.

Acknowledgements

This work was supported by the National Key Research and Development Program of China (Grant number 2016YFC0802800) and the National Natural Science Foundation of China (Grant number 51606011 and 51874041). The fourth author acknowledges the support from Australian Research Council via Discovery Early Career Researcher Award (Grant number DE160101116). Fan Tang and Yanlong Sun contributed equally in this work.

References

[1] J. Kadkhodapour, H. Montazerian, M. Samadi, S. Schmauder, A.A. Mehrizi, Plastic deformation and compressive mechanical properties of hollow sphere aluminum foams produced by space holder technique, Mater. Des. 83 (2015) 352–362.
[2] J. Fan, J. Zhang, Z. Wang, Z. Li, L. Zhao, Dynamic crushing behavior of random and functionally graded metal hollow sphere foams, Mater. Sci. Eng. A 561 (3) (2013) 352–361.
[3] W.S. Sanders, L.J. Gibson, Mechanics of hollow sphere foams, Mater. Sci. Eng. A 347 (1) (2003) 70–85.
[4] S. Ahmed, K. Galal, Effectiveness of FRP sandwich panels for blast resistance, Compos. Struct. 163 (2017) 454–464.
[5] A. Szlancsik, B. Katona, K. Bobor, K. Májlinger, I.N. Orbulov, Compressive behaviour of aluminium matrix syntactic foams reinforced by iron hollow spheres, Mater. Des. 83 (2015) 230–237.
[6] K. Mohan, T.H. Yip, S. Idapalapati, Z. Chen, Impact response of aluminum foam core sandwich structures, Mater. Sci. Eng. A 529 (1) (2011) 94–101.
[7] C. Qi, A. Remennikov, L.Z. Pei, S. Yang, Z.H. Yu, T.D. Ngo, Impact and close-in blast response of auxetic honeycomb-cored sandwich panels: experimental tests and numerical simulations, Compos. Struct. 180 (2017) 161–178.
[8] J.H. Choi, S.J. Choi, J.H.J. Kim, K.N. Hong, Evaluation of blast resistance and failure behavior of prestressed concrete under blast loading, Constr. Build. Mater. 173 (2018) 550–572.
[9] A. Gargano, K. Pingkarawat, V.L. Pickerd, M.E. Ibrahim, A.P. Mouritz, Effect of fibre-matrix interfacial strength on the explosive blast resistance of carbon fibre laminates, Compos. Sci. Technol. 138 (2016) 68–79.
[10] G.S. Langdon, D. Karagiozova, M.D. Theobald, G.N. Nurick, G. Lu, R.P. Merrett, Fracture of aluminium foam core sacrificial cladding subjected to air-blast loading, Int. J. Impact Eng. 37 (6) (2010) 638–651.
[11] S. Gasser, F. Paun, Y. Bréchet, Finite elements computation for the elastic properties of a regular stacking of hollow spheres, Mater. Sci. Eng. A 379 (1) (2004) 240–244.
[12] M. Vesenjak, Z. Ren, T. Fiedler, A. Oechsner, Impact behavior of composite hollow sphere structures, J. Compos. Mater. 43 (22) (2009) 2491–2505.
[13] H.B. Zeng, S. Pattofatto, H. Zhao, Y. Girard, V. Fascio, Impact behaviour of hollow sphere agglomerates with density gradient, Int. J. Mech. Sci. 52 (5) (2010) 680–688.
[14] P. Li, N. Petrinic, C.R. Siviour, Finite element modelling of the mechanism of deformation and failure in metallic thin-walled hollow spheres under dynamic compression, Mech. Mater. 54 (2012) 43–54.
[15] B.H. Smith, S. Szyniszewski, J.F. Hajjar, B.W. Schafer, S.R. Arwade, Characterization of steel foams for structural components, Metals 2 (4) (2012) 399–410.

[16] I. Shufrin, E. Pasternak, A.V. Dyskin, Negative Poisson's ratio in hollow sphere materials, Int. J. Solids Struct. 54 (2015) 192–214.
[17] S. Yang, G. Liu, Q. Chang, D. Wang, Simulation and optimization for anti-shock performances of graded metal hollow sphere foam structure, Journal of Zhejiang University (Engineering Science) 50 (8) (2016) 1593–1599.
[18] J. Song, Q. Sun, Z. Yang, S. Luo, X. Xiao, S.R. Arwade, G. Zhang, Effects of microporosity on the elasticity and yielding of thin-walled metallic hollow spheres, Mater. Sci. Eng. A 688 (2017) 134–145.
[19] C. Qi, S. Yang, L.J. Yang, Z.Y. Wei, Z.H. Lu, Blast resistance and multi-objective optimization of aluminum foam-cored sandwich panels, Compos. Struct. 105 (8) (2013) 45–57.
[20] H. Liu, Z.K. Cao, G.C. Yao, H.J. Luo, G.Y. Zu, Performance of aluminum foam-steel panel sandwich composites subjected to blast loading, Mater. Des. 47 (9) (2013) 483–488.
[21] G. Imbalzano, S. Linforth, T.D. Ngo, P.V.S. Lee, P. Tran, Blast resistance of auxetic and honeycomb sandwich panels: comparisons and parametric designs, Compos. Struct. 183 (2017) 242–261.
[22] R.P. Merrett, G.S. Langdon, M.D. Theobald, The blast and impact loading of aluminium foam, Mater. Des. 44 (2013) 311–319.
[23] N. Lam, P. Mendis, T. Ngo, Response spectrum solutions for blast loading, Electron. J. Struct. Eng. 4 (4) (2004) 28–44.
[24] D. Jenson, V.U. Unnikrishnan, Energy dissipation of nanocomposite based helmets for blast-induced traumatic brain injury mitigation, Compos. Struct. 121 (2015) 211–216.
[25] M. Van der Voort, K.B. Holm, P. Kummer, J.A. Teland, J. Van Doormaal, H. Dijkers, A new standard for predicting lung injury inflicted by Friedlander blast waves, J. Loss Prev. Process Ind. 40 (2016) 396–405.
[26] A. Bravais, On the Systems Formed by Points Regularly Distributed on a Plane or in Space, Crystallographic Society of America, Washington, 1949.
[27] W.S. Sanders, L.J. Gibson, Mechanics of BCC and FCC hollow-sphere foams, Mater. Sci. Eng. A 352 (1–2) (2003) 150–161.
[28] V. Marcadon, Mechanical modelling of the creep behaviour of hollow-sphere structures, Comput. Mater. Sci. 50 (10) (2011) 3005–3015.
[29] V.M. Thanh, S.P. Santosa, D. Widagdo, I.S. Putra, Steel plate behavior under blast loading-numerical approach using LS-DYNA, Appl. Mech. Mater. 842 (2016) 200–207.
[30] S. Bagherifard, N. Beretta, S. Monti, M. Riccio, M. Bandini, M. Guagliano, On the fatigue strength enhancement of additive manufactured AlSi10Mg parts by mechanical and thermal post-processing, Mater. Des. 145 (2018) 28–41.
[31] J. Wu, L. Wang, X. An, Numerical analysis of residual stress evolution of AlSi10Mg manufactured by selective laser melting, Optik-International Journal for Light and Electron Optics 137 (2017) 65–78.
[32] F. Zhu, L. Zhao, G. Lu, Z. Wang, Structural response and energy absorption of sandwich panels with an aluminium foam core under blast loading, Adv. Struct. Eng. 11 (5) (2008) 525–536.
[33] V.A. Phadnis, P. Kumar, A. Shukla, A. Roy, V.V. Silberschmidt, Optimising curvature of carbon fibre-reinforced polymer composite panel for improved blast resistance: finite-element analysis, Mater. Des. 57 (5) (2014) 719–727.
[34] M.S.H. Fatt, H. Surabhi, Blast resistance and energy absorption of foam-core cylindrical sandwich shells under external blast, Compos. Struct. 94 (11) (2012) 3174–3185.
[35] W. Chen, H. Hao, S. Chen, F. Hernandez, Performance of composite structural insulated panel with metal skin subjected to blast loading, Mater. Des. 84 (2015) 194–203.
[36] G. Imbalzano, P. Tran, T.D. Ngo, P.V.S. Lee, A numerical study of auxetic composite panels under blast loadings, Compos. Struct. 135 (2016) 339–352.
[37] X. Liu, X. Tian, T.J. Lu, D. Zhou, B. Liang, Blast resistance of sandwich-walled hollow cylinders with graded metallic foam cores, Compos. Struct. 94 (8) (2012) 2485–2493.
[38] M.D. Theobald, G.S. Langdon, G.N. Nurick, S. Pillay, A. Heyns, R.P. Merrett, Large inelastic response of unbonded metallic foam and honeycomb core sandwich panels to blast loading, Compos. Struct. 92 (10) (2010) 2465–2475.
[39] R. SRIRAM, U.K. VAIDYA, J.E. KIM, Blast impact response of aluminum foam sandwich composites, J. Mater. Sci. 41 (13) (2006) 4023–4039.
[40] L. Jing, Z. Wang, L. Zhao, Dynamic response of cylindrical sandwich shells with metallic foam cores under blast loading-numerical simulations, Compos. Struct. 99 (5) (2013) 213–223.
[41] X. Li, P. Zhang, Z. Wang, G. Wu, L. Zhao, Dynamic behavior of aluminum honeycomb sandwich panels under air blast: experiment and numerical analysis, Compos. Struct. 108 (1) (2014) 1001–1008.
[42] J. Zhou, G. Tao, The mechanical properties for the attenuation of shock wave interaction with watery foam material, Adv. Mater. Res. 815 (2013) 558–566.